Wireless Pers. Commun. manuscript No.
(will be inserted by the editor)

Reconsideration of Optimal Carrier Sensing in Distributed Control Wireless Ad Hoc Networks

Mayur M. Vegad · Swades De · Brejesh Lall

Received: date / Accepted: date

Abstract IEEE 802.11 wireless ad hoc network performance in DCF (distributed coordination function) mode is limited by hidden and exposed terminals problem. RTS/CTS (request-to-send/clear-to-send) based hand shake reduces the problem to some extent, but the network performance is a function of nodal carrier sense (CS) range and interference range. While a large CS range compared to the interference range can reduce the collision related throughput loss, it has a negative impact of increased exposed terminals.

Via experimental studies it was recently demonstrated that, the effect of interference to a reception process differs depending on arrival order of the desired signal and interfering signal. In view of this frame arrival order dependent capture (ODC) capability of receivers, in this paper we investigate the optimal choice of CS range and explore the possibility of maximizing the network performance. Via mathematical analysis, supported by extensive network simulations, we demonstrate the network performance benefit of ODC dependent optimal CS range. The distinctive characteristic of ODC diminishes at higher data rates, and as a result the performance gain with optimal CS range reduces. Nevertheless, at low-to-moderately-high data rates, the performance gain is shown to be quite significant.

Keywords Medium access control · optimal carrier sensing · order dependent capture · mathematical modeling · hidden terminals · exposed terminals

1 Introduction

Medium access control (MAC) protocol plays an important role of coordinating the users' access to the shared medium in wireless networks. Though, IEEE 802.11 [4] is a standard protocol suit for the wireless local area networks (LANs), its distributed coordination function (DCF) has also been studied and widely adopted in wireless ad hoc networks. DCF is a kind of CSMA/CA (carrier sense multiple access with collision avoidance) MAC protocol wherein the carrier sensing (CS) is the fundamental aspect. Each user senses the medium before making a transmission attempt and defers the transmission if the medium is sensed busy. The 802.11 suggests two types of CS: physical carrier sensing (PCS) and virtual carrier sensing (VCS). In PCS, the medium is determined to be busy if the signal power is larger than a threshold called CS threshold Γ_c; otherwise it is considered idle. A given value of threshold Γ_c determines the corresponding CS range R_c which is the minimum distance allowed between two concurrent transmitters. In VCS, each user regards the channel as busy for the duration mentioned in the MAC header of the received frames, such as, RTS (request to send), CTS (clear to send), Data, and ACK

M. M. Vegad
Electrical Engineering Department, Indian Institute of Technology Delhi, New Delhi, India
E-mail: mayur8374@gmail.com

S. De
Electrical Engineering Department, Indian Institute of Technology Delhi, New Delhi, India
E-mail: swadesd@ee.iitd.ac.in

B. Lall
Electrical Engineering Department, Indian Institute of Technology Delhi, New Delhi, India
E-mail: brejesh@ee.iitd.ac.in

(acknowledgment) [4]. One objective of CS (both PCS and VCS) is to cover possible interferers in the sensing range so as to avoid collisions. A potential interferer left uncovered by CS is called a hidden terminal.

The interfering range R_i (within which a transmitted frame can cause collision to an ongoing reception) around a receiver increases with the sender-receiver separation distance d. Therefore, one way to reduce the hidden regions is to keep d small, so that the farthest potential interferer is covered within a given CS range of the sender [26]. Alternatively, one may increase the value of CS range R_c [8] so as to cover the farthest possible interferer for the largest value of d (= the nodal transmission range, R_t). But, this approach may not be preferable, as it increases the number of exposed terminals, and hence reduces the spatial reuse. This negative impact becomes quite significant at high data rates because of increase in R_i with the data rates. Increasing the CS threshold Γ_c (thereby reducing R_c) arbitrarily would solve the exposed terminals problem but at the cost of increasing the hidden terminals problem. The excessive collisions due to hidden terminals result in false link/route failure alarms, resulting in unnecessarily triggering the corresponding recovery mechanisms at routing and transport layers. This, in turn, either increases network traffic by flooded broadcast packets or slows down some flows to starvation, creating unfairness amongst the competing flows. Thus, there is some tradeoff and the value of Γ_c (and hence R_c) must be set optimally so as to have a favorable balance between desired spatial reuse and allowable interference.

When more than one frames are received at a receiver in overlapped fashion, one of them can be successfully decoded if the signal-to-interference (SIR) ratio is above a threshold, called capture threshold δ. While the dependence of δ on data rate and other physical parameters, such as the modulation scheme, are well known, recent experimental results [11], [21] have shown that, the value of δ also depends on the arrival order of the overlapping frames. Particularly, for data rates up to 18 Mbps, δ is significantly small when the intended frame arrives earlier than an interfering frame (**S**ender's **F**irst, or SF case), otherwise it is large (**S**ender's **L**ast, or SL case). The SF case leads to a much smaller value of R_i around a node that has started receiving a signal. This SF/SL phenomenon motivates us to take into account the frame arrival order dependent capture (ODC) while considering the optimization of CS threshold, so as to increase the network throughput.

There have been significant prior research works (e.g., [6], [27], [31], [32]) that suggest different approaches towards the optimization of the CS threshold to achieve enhanced network performance. On the other hand, a few researchers [23], [21] have proposed exploiting ODC at the physical layer (PHY) for improving the network performance by reordering the transmissions at the MAC layer. To the best of our knowledge, no work has been reported in the literature that studies the role of ODC in the optimization of CS threshold.

Note that, the value of δ is still higher in SL cases, and it may appear that the step of arbitrarily reducing R_c involves a risk of leaving the fate (success/failure) of a transmitted frame to pure chance. That is, a frame will be successful, only if it is received either in isolation or in SF overlap fashion. But actually, the VCS plays a significant role. In our prior work [25] we have shown that, once the RTS/CTS exchange is successful, the interfering range in SL case is reduced significantly. By analyzing various possible overlapping cases it was shown that, with ODC at PHY it is possible to safely reduce the CS range. However, the claims in [25] were purely based on simulations and lacked any theoretical justification. Moreover, the evaluation was carried out only at the basic (1 Mbps) data rate of 802.11b.

In this paper, we develop an analytical framework to characterize the impact of ODC in optimizing the CS threshold at different data rates of IEEE 802.11a. The key contributions of this work are as follows: (a) An analytical model is developed with ODC at PHY for the RTS/CTS based access scheme of IEEE 802.11 standard, and the results are supported by rigorous ns2 simulations; (b) the significance of considering ODC on the CS threshold decision at the MAC layer is demonstrated through numerical results at different data rates of IEEE 802.11a.

The remaining paper is organized as follows: Section 2 surveys the related works. After building some background on nodal ranges and order dependent capture capability in Section 3, we develop the analytical model with incorporation of ODC in Section 4. In Section 5, we validate the model through network simulations in ns2. In Section 6, we use the developed analytical model to evaluate the impact of ODC on the consideration of PCS threshold at different data rates of IEEE 802.11a. Finally, Section 7 concludes the paper.

2 Related Works

Improving spatial reuse through variations of VCS: Some researchers [26], [28], [14] have proposed to improve spatial reuse through some variations in the VCS mechanism while assuming a fixed PCS threshold. Depending upon the value of δ, one can define a critical sender-receiver distance d beyond which the R_i becomes larger than the R_t. For a d larger than the critical distance, the above phenomenon makes the RTS/CTS ineffective in mitigating the hidden terminals that are located outside the transmission range. To solve this problem, it was proposed

in [26] that a RTS is responded only if it is received from a distance that is lower than the critical distance. As per the basic IEEE 802.11 standard, every node respects all the overheard frames by deferring its own transmissions until the duration mentioned in the overheard frames. Targeting improved spatial reuse through mitigation of exposed terminals, the authors in [28] suggested that a node needs to respect an overheard RTS or CTS only if it is received in isolation (i.e., only RTS or only CTS). It can be shown that, while their approach works better for a smaller d, the throughput performance significantly deteriorates as d increases. When an overheard frame is erroneous (or sensed only), the exact duration by which a node should defer its transmission may not be known. In such a case, according to the basic IEEE 802.11 standard a node defers blindly for a fixed duration (represented by extended inter-frame space or EIFS) without discriminating amongst the different types of overheard frames. An enhanced carrier sensing approach in [14] distinguishes among the types of erroneous frames based on their lengths, and thus it allows the overhearing nodes to defer their transmissions accordingly. None of [26], [28], and [14] considered ODC at PHY.

Tuning of CS threshold: Several researchers [6], [27], [31], [32], [19], [24] have recommended tuning of PCS threshold in order to achieve a trade-off between the amount of spatial reuse and probability of frame collisions, though none of them have considered the role of ODC in their works. Perhaps, [6] was the first to suggest the tuning of PCS threshold against the fixed one, which was assumed in earlier works [26], [14] and is being used widely in some network simulators [3]. The authors in [27] argued for accounting bandwidth independent and bandwidth dependent MAC overhead while determining an optimal Γ_c. In [31] it was demonstrated that, PCS enhanced with tunable Γ_c can avoid interference, thereby obviating the need of VCS altogether. The analytical model in [32] computed an optimal PCS threshold and also suggested a PCS tuning algorithm for adapting the PCS threshold to varying network conditions. In [18], the authors proposed an algorithm that differentiates the packet losses due to hidden and non-hidden interferers and tunes PCS adaptively. The analytical model in [19] showed that, a close-to-optimal CS range is equal to the interference range R_i. To achieve a control over variable R_i in practical networks (where d is random), they proposed a rate-to-link allocation scheme based on rendering the R_i equal for all links, allowing a single CS range to be used in the whole network. The effect of PCS on multi-rate and multi-hop wireless ad hoc networks was studied in [29]. In determining an optimal Γ_c, they considered several factors, like variable transmission ranges and receiver sensitivities for different data rates, impact of multi-hop forwarding, node topology, and bidirectional handshake. The authors in [30] have distinguished the SL and SF type of collisions (calling them H_1 and H_2 collisions, respectively) and discusses solutions to each of these types. In [24], the authors use the framework of IEEE 802.11k *Radio Resource Management* on each node to enable online tuning of CS threshold.

Spatial reuse through power control: The level of spatial reuse can also be enhanced by reducing the level of transmit power. To improve spatial reuse, the experimental study in [9] presented an interesting comparison of two approaches, namely, tuning of transmit power and CS threshold. Similarly, the analytical model in [15] addressed the joint tuning of PHY (transmit power and data rate) and MAC (contention window size) parameters to optimize the network throughput by determining appropriate data rate for a given signal-to-interference-and-noise ratio (SINR). These works however, did not exploit ODC at PHY.

Experimentation and exploitation of ODC: Usefulness of capture capability in IEEE 802.11 based wireless networks was experimentally evaluated in [10], [11]. Particularly, the *Message-in-Message* feature of modern wireless receivers and the corresponding ODC effect at various data rates of IEEE 802.11a was studied by [11], [12], [21] through test-bed experimentations. At low data rates, for very small sender-receiver separation distances, the interference range can be smaller than the communication range. Observing this fact, the study in [23] exploited the ODC to effect concurrent transmissions even within a communication range through *properly staggering* the different transmissions. This approach however requires a considerable modification in the existing 802.11 MAC. Further, it did not consider the role of CS range, and hence the exposed terminals that are out of communication range of the sender and receiver were not addressed. Through another set of test-bed experiments the authors in [21] emphasized the importance of frame reception order (SF versus SL) and proposed a link layer protocol that achieves ODC aware *reordering* of transmissions for optimal network throughput. The analytical study in [**?**] has quantified the gains from the concurrency made possible by exploiting MIM-capture in IEEE 802.11 WLANs. ODC has also been studied experimentally in wireless sensor networks (WSNs) [16,**?**]. In [16] Lu et al. have shown that due to the concurrent transmissions made possible by the capture effect, it is possible to expedite the network flooding in WSNs. The authors in [20] suggest a new MAC layer protocol for WSNs based on MIM-capture that allows parallel transmissions leading to enhanced throughput and reduced power consumption.

To complement the prior studies, in our work we aim at increasing the spatial reuse, and as a result network throughput, by judiciously exploiting the ODC in determining the optimal CS range. In contrast to the approach in

[23], our approach does not impose any restriction on the sender-receiver distance. We also develop a mathematical model to quantify the impact of ODC on the choice of CS threshold.

3 Background Concepts

We develop some background to appreciate the analytical treatment in the following section.

3.1 Nodal Ranges

Transmission range R_t and CS range R_c: When a sender **S** transmits a frame with power P_T, following standard path loss model [22], the received signal strength P_r at a receiver **R** is given as:

$$P_r = P_0 \left(\frac{d_0}{d_{SR}} \right)^{\alpha}, \tag{1}$$

where P_0 is the received signal strength measured at a reference distance d_0, d_{SR} indicates the separation distance of nodes **S** and **R**, and α is the path loss exponent (usually $2 \leq \alpha \leq 4$).

Let Γ_t be the minimum power level required for successful decoding of a received frame. Then the distance from the transmitter at which, the received signal strength equals Γ_t is called the transmission range R_t. Using (1) it can be given as

$$R_t = d_0 \left(\frac{P_0}{\Gamma_t} \right)^{\frac{1}{\alpha}}. \tag{2}$$

In a CSMA/CA MAC protocol (e.g., DCF of IEEE 802.11), all the participating nodes follow *listen before talk* policy and ensures the availability of medium before using it for its own transmission. To this end, besides Γ_t, each node maintains another threshold called CS threshold Γ_c. When the sensed power level is above Γ_c, the medium is identified as busy and a transmission aspirant node defers its own transmission [4]. This leads to a definition of CS range R_c around the transmitter which is the minimum distance between two permitted concurrent transmissions. From (1),

$$R_c = d_0 \left(\frac{P_0}{\Gamma_c} \right)^{\frac{1}{\alpha}}. \tag{3}$$

Since, P_0 is proportional to the transmit power P_T, R_t and R_c are also the functions of P_T as well as of the respective thresholds.

Interference Range R_i: For a successful frame reception, the SIR at **R** should be above a capture threshold δ. Let P_s and P_i be the respective signal strengths from sender **S** and interferer **I** at **R**. Under the assumption of homogeneous transmit power being used for all (data and control) frames at all participating nodes, from (1) the minimum SIR condition can be given as:

$$\frac{P_s}{P_i} = \left(\frac{d_{IR}}{d_{SR}} \right)^{\alpha} \geq \delta. \tag{4}$$

The condition in (4) gives us the interference range R_i. Therefore,

$$R_i = (\delta)^{\frac{1}{\alpha}} \cdot d_{SR} = K \cdot d_{SR}, \tag{5}$$

where $K \triangleq \delta^{\frac{1}{\alpha}}$. Thus, $R_i \propto d_{SR}$ and is maximum when $d_{SR} = R_t$. That is,

$$R_{i_{max}} = K \cdot R_t. \tag{6}$$

From (5) it is clear that, when $K > 1$, even for a moderately large value of d_{SR} the interference range can be larger than the transmission range.

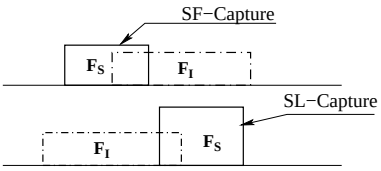

Fig. 1 SF and SL overlaps. F_S and F_I are signal and interfering frames, respectively. Note that, the signal power of F_S required for signal capture in SF case is lower than that in SL case.

3.2 Order Dependent Capture (ODC)

Interference in wireless networks can be better handled with *message-in-message* (MIM) feature of modern wireless receivers [1]. The test-bed experimental studies with MIM-capable wireless nodes have found that the value of capture threshold δ depends on order of arrival of the overlapping frames [11,12,21]. This dependence is in addition to the employed data rate and other physical parameters (such as modulation scheme). Fig. 1 shows two possible frame arrival orders: **S**ender's **F**irst SF case and **S**ender's **L**ast SL case. It was experimentally found in [11,12,21] that, the value of δ differs in the above two cases, the difference being larger at low data rates. The reference values of δ for SF and SL cases[1] at different data rates are depicted in Table 1.

Table 1 The values of δ for SF and SL cases at different data rates of IEEE 802.11a [11,12]

Data rate (Mbps)	**6**	**9**	**12**	**18**	**24**	**36**	**48**	**54**
δ^{SF} (dB)	0	3	4	7	11	15	21	23
δ^{SL} (dB)	10	10	10	10	12	16	22	23

4 Analytical Model for RTS/CTS Access Scheme of IEEE 802.11

We consider a network with N users deployed over a two dimensional (2-D) plane obeying homogeneous spatial Poisson distribution with node density λ. Each data frame is preceded with RTS/CTS exchange. Saturated traffic scenario is considered where all nodes have always a data packet to transmit. The model assumes no action by upper layers in response to the MAC failures. CTS and ACK packets are transmitted by a receiver after successfully receiving RTS and data frames, respectively. Further, both of these control packets are very small and transmitted at the lowest (reliable) data rate. So, our model neglects the loss probabilities of CTS and ACK frames.

In IEEE 802.11 standard, when a node finds the channel busy, it freezes its back-off counter. This leads to a variable time interval between two consecutive time slot beginnings. Hence, it is convenient to define a generic time slot T_{gen} [5], which could be much longer than the system time slot. In the subsequent developments, we use only 'time slot' to refer to the generic time slot.

4.1 Description of state model

The basic (without RTS/CTS) access scheme of IEEE 802.11 can be captured in an analytical node level model consisting of following 4 states: Idle (node is idle), DATA-Success (node is engaged in a successful transmission attempt), DATA-Failure (node is engaged in an unsuccessful transmission attempt), or Deferring (node is deferring due to busy medium reported by PCS) [17]. In our work we need to develop a model for RTS/CTS based access scheme. The prior exchange of two small frames (i.e., RTS, CTS) leads to a behavior of a node that is much more complex than that in case of the basic access scheme. Consequently, the corresponding analytical model needs 3 more states to capture the behavior of a generic node.

Fig. 2 shows the resulting 7-state node level model which is constructed from the perspective of a generic reference node $\mathbf{n}_0$ in the system. In a given time slot, $\mathbf{n}_0$ can be in any of the following 7 states:

[1] Besides SF and SL overlap cases, the authors in [11] have also experimented with a third possible case (called SLG capture case) where the first arriving frame (from the interferer) is already *garbled*. Because of relatively less probability of such overlaps, we do not consider SLG capture case in our work.

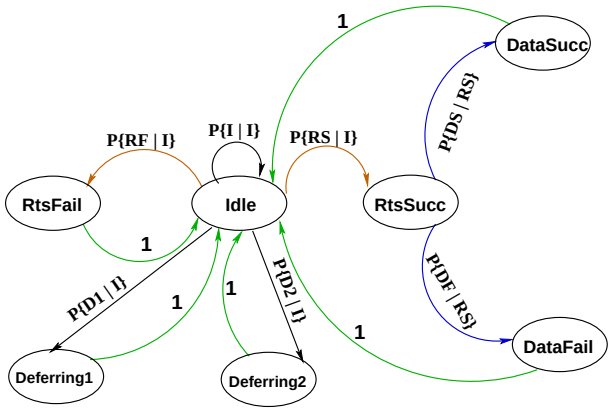

Fig. 2 A 7-state nodal model for RTS/CTS access scheme of IEEE 802.11.

Idle (I) State: A node remains in Idle state if neither the $\mathbf{n}_0$ node nor any other node in its CS range transmits. The duration T_I, for which $\mathbf{n}_0$ stays in the Idle state, is the length of system time slot defined in IEEE 802.11 standard (e.g., in 802.11a, $T_I = 9\mu S$).

RTS-Success (RS) State: $\mathbf{n}_0$ node transmits a RTS frame which is successfully responded with a CTS from its intended receiver. If a transmission attempt by $\mathbf{n}_0$ results in a successful response of CTS by the intended receiver, it transits from Idle state to RTS-Success state. Here, the success of a RTS frame requires for both of the following events to occur: (i) RTS is not lost in collisions at the receiver, and (ii) The network allocation vector (NAV) [4] of receiver is zero when the RTS is received. The duration (in micro seconds or μS), for which a node stays in this state is given as:

$$T_{RS} = T_{RTS} + SIFS + \sigma + T_{CTS} + DIFS + \sigma \ \ \mu\text{S},$$

where σ is the propagation delay. In 802.11a, T_{RTS} and T_{CTS} are calculated as:

$$T_{RTS} = 20 + 4\left\lceil \frac{182}{4\nu_h} \right\rceil \mu\text{S}, \text{ and } \ T_{CTS} = 20 + 4\left\lceil \frac{134}{4\nu_h} \right\rceil \mu\text{S}.$$

where ν_h is control frame transmission rate in Mbps.

RTS-Failure (RF) State: $\mathbf{n}_0$ transmits a RTS frame which is not responded with a CTS from its intended receiver. If a RTS transmission does not get a CTS in response, the node transits from Idle to RTS-Failure state. Here, a RTS failure implies occurrence of any of the following events: (i) RTS is lost in collisions at the receiver, or (ii) The NAV of receiver is non-zero when the RTS is received. Before confirming the non-reception of a valid CTS frame, $\mathbf{n}_0$ waits for a timeout period which is almost equal to the transmission time of a CTS frame [4]. Therefore, $T_{RF} \approx T_{RS} \ \ \mu\text{S}$.

DATA-Success (DS) State: After successful reception of CTS, $\mathbf{n}_0$ transmits data frame and receives an ACK successfully from the receiver. For such scenarios, $\mathbf{n}_0$ moves from RTS-Success to Data-Success state. This implies that, data frame reaches the receiver without any collisions. Recall that, we have assumed that ACK collisions are negligible [2]. The duration of this state is

$$T_{DS} = T_{data} + SIFS + \sigma + T_{ACK} + SIFS + \sigma \ \ \mu\text{S}.$$

The time durations of a data frame T_{data} and an ACK frame T_{ACK} can be derived as:

$$T_{data} = 20 + 4\left\lceil \frac{294 + L_{dt}}{4\nu} \right\rceil \mu\text{S}, \text{ and } \ T_{ACK} = 20 + 4\left\lceil \frac{134}{4\nu_h} \right\rceil \mu\text{S},$$

where L_{dt} (in bits) is length of data frame and ν is the data frame transmission rate in Mbps.

DATA-Failure (DF) State: After successful reception of CTS, $\mathbf{n}_0$ transmits data frame but does not receive an ACK from the receiver. Here, $\mathbf{n}_0$ transitions from RTS-Success state to Data-Failure state. This happens when the data frame is lost in collision at the receiver. Before confirming the non-reception of a valid ACK frame, $\mathbf{n}_0$ waits for a timeout period which is almost equal to the transmission time of an ACK frame [4]. Thus, $T_{DF} \approx T_{DS} \ \ \mu\text{S}$.

[2] Also note that, as per IEEE 802.11 standard [4], having received a data frame successfully, a receiver sends the ACK without any type of carrier sensing, neither PCS nor VCS.

Deferring-1 (D1) State: In a time slot the node $\mathbf{n}_0$ transitions from Idle to this state if in that time slot $\mathbf{n}_0$ itself does not initiate a transmission but it starts receiving a RTS frame for the case when the RTS/CTS exchange results in a successful data transmission. It results in a successful communication session consisting of the complete 4-way exchange of RTS-CTS-data-ACK between a sender-receiver pair, for which both or at least the sender is located in its CS range. Note that, this completes the reception aspect of $\mathbf{n}_0$ as well. The duration in this state is: $T_{D_1} = T_{RS} + T_{DS}$ μS.

Deferring-2 (D2) State: In a time slot the node $\mathbf{n}_0$ transitions from Idle to this state if in that time slot, $\mathbf{n}_0$ itself does not initiate a transmission but, starts receiving a RTS frame, either destined to itself or an overheard frame, and for the case when this RTS results in to a failure. The duration for which $\mathbf{n}_0$ stays in this state can be obtained as follows. If the received RTS is decoded successfully at $\mathbf{n}_0$, then according to IEEE 802.11 standard, $\mathbf{n}_0$ will update its NAV and respectfully defer for a duration mentioned in the RTS frame irrespective of the consequences (success or failure) of that RTS, and hence, $T_{D_2} = T_{D_1}$. However, if a failed (decodable) RTS was destined to $\mathbf{n}_0$ then $T_{D2} = T_{RF} \approx T_{RS}$. Further, if a failed RTS was received as a 'sensed only' frame at $\mathbf{n}_0$, then according to the *EIFS mechanism*, $T_{D_2} = T_{RTS} + EIFS \approx T_{RS}$. To simplify the analysis we take only one value of the duration as: $T_{D_2} = T_{RS}$ μS.

To derive the steady state and transition probabilities, let Π_S denote the steady state probability of state S and $P\{S_2|S_1\}$ denote a transition probability from state S_1 to state S_2. Then each of the steady state probabilities can be described in terms of the steady state probability of Idle state as:

$$\Pi_{RS} = \Pi_I P\{RS|I\}, \tag{7a}$$
$$\Pi_{RF} = \Pi_I P\{RF|I\}, \tag{7b}$$
$$\Pi_{DS} = \Pi_{RS} P\{DS|RS\} = \Pi_I P\{RS|I\} P\{DS|RS\}, \tag{7c}$$
$$\Pi_{DF} = \Pi_{RS} P\{DF|RS\} = \Pi_I P\{RS|I\} P\{DF|RS\}, \tag{7d}$$
$$\Pi_{D1} = \Pi_I P\{D1|I\}, \tag{7e}$$
$$\Pi_{D2} = \Pi_I P\{D2|I\}. \tag{7f}$$

Assuming time-homogeneity of the Markov chain in Fig. 2, we have for the idle state: $\Pi_I = P\{I|I\}\Pi_I + P\{I|RF\}\Pi_{RF} + P\{I|D1\}\Pi_{D1} + P\{I|D2\}\Pi_{D2} + P\{I|DS\}\Pi_{DS} + P\{I|DF\}\Pi_{DF}$. Observing that a node moves to Idle from RF, D1, D2, DS, and DF with probability 1, we obtain:

$$\Pi_I = P\{I|I\}\Pi_I + \Pi_{RF} + \Pi_{D1} + \Pi_{D2} + \Pi_{DS} + \Pi_{DF}. \tag{8}$$

Substitutions from (7b) to (7f) into (8) and simplification yields

$$P\{I|I\} + P\{RF|I\} + P\{RS|I\}\left(P\{DS|RS\} + P\{DF|RS\}\right) + P\{D1|I\} + P\{D2|I\} = 1. \tag{9}$$

The model also assumes, after receiving a CTS successfully a node always transmits a data frame, which results either in a success or a failure, i.e.,

$$P\{DS|RS\} + P\{DF|RS\} = 1 \tag{10}$$

Further, we denote τ_R as the probability of RTS transmission by any node from its Idle state. So,

$$\tau_R = P\{RS|I\} + P\{RF|I\} \tag{11}$$

Using substitutions from (10) and (11), (9) simplifies to

$$P\{I|I\} + \tau_R + P\{D1|I\} + P\{D2|I\} = 1. \tag{12}$$

For simplicity, we assume no retransmission of RTS or data. This implies no exponential backoff in DCF and hence, use of a fixed contention window CW. Therefore, τ_R is given as [5]:

$$\tau_R = \frac{2}{CW + 1}. \tag{13}$$

Since the channel is shared with all neighbors of the reference node $\mathbf{n}_0$, the status of surrounding nodes is required to be considered while computing the transition probabilities. When every node in the network is within the CS range of every other node (as assumed in [5]), all nodes in the CS range of $\mathbf{n}_0$ perceive the channel status same as $\mathbf{n}_0$, and hence, it is reasonable to consider that, the RTS-transmission probability of all neighbors, given they are in Idle state, is the same (i.e., τ_R). Note that, this is possible only if all nodes are at the same physical location or

if the CS range of each node is large enough to cover the farthest node in the system. When such is not the case, the network environment (or the channel status) 'seen' by one node greatly differs from the one 'seen' by other node. Further, with increasing distances between them or with reducing CS range (or with both), the difference between their channel status becomes pronounced because of their large non-overlapping CS regions. Therefore, the RTS-transmission probability ρ in the next time slot of these nodes cannot be taken same as that of $\mathbf{n}_0$. Rather, it has to be computed as the average RTS-transmission probability per generic slot derived as:

$$\rho = \Pi_{RS} + \Pi_{RF} = \Pi_I \tau_R. \tag{14}$$

To compute the transition probabilities of our model, as in [17] we consider that, when the channel around node $\mathbf{n}_0$ is sensed Idle, the nodes within the transmission range of $\mathbf{n}_0$ share the same channel status and hence, have the same RTS-transmission probability τ_R. On the other hand, the status of other CS range neighbors that are outside the transmission range of $\mathbf{n}_0$ is independent of the status of $\mathbf{n}_0$ and hence, they transmit RTS with generic RTS-transmission probability ρ.

Note that, at any instant the node can be in any one of the seven states. So,

$$\Pi_I + \Pi_{DS} + \Pi_{DF} + \Pi_{RS} + \Pi_{RF} + \Pi_{D1} + \Pi_{D2} = 1. \tag{15}$$

Substituting from (7a) to (7f) in (15), and subsequently using (10) and (11), we get

$$\Pi_I = \frac{1}{(1 + P\{RS|I\} + \tau_R + P\{D1|I\} + P\{D2|I\})} \ . \tag{16}$$

The generic slot time can be derived as: $T_{gen} = \Pi_I T_I + \Pi_{DS} T_{DS} + \Pi_{DF} T_{DF} + \Pi_{RS} T_{RS} + \Pi_{RF} T_{RF} + \Pi_{D1} T_{D1} + \Pi_{D2} T_{D2}$. Using (7a)-(7f), (10), and (11), and substituting $T_{DS} = T_{DF}$, $T_{RS} = T_{RF} = T_{D2}$ and $T_{D1} = T_{RS} + T_{DS}$ we get,

$$T_{gen} = \Pi_I \big(T_I + T_{DS}(P\{RS|I\} + P\{D1|I\}) + T_{RS}(\tau_R + P\{D1|I\} + P\{D2|I\})\big). \tag{17}$$

In the following, we determine the probability of receiving a CTS in response to a RTS frame.

4.2 Analysis of Success/Failure of RTS Frame

A transmitted RTS may not be responded with a CTS by its intended receiver for two reasons. First, the RTS may be lost due to collision, and second, the receiver may not respond to RTS because it finds the channel not available. Hence, we investigate the collision vulnerability of RTS frame and also determine the probability that a RTS is not responded with a CTS. Eventually, we obtain an equation for probability of successful RTS transmission.

4.2.1 Collisions of a RTS frame

A RTS frame is said to be lost due to collision if it is received at the receiver in overlapped fashion with another frame being transmitted from within interference range of the receiver. Accordingly, all the nodes within the interference range of node **R** are potential interferers in Fig. 3.

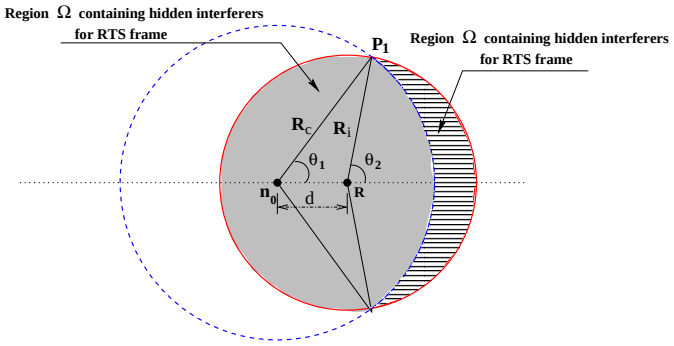

Fig. 3 The nodes in the horizontal-dashed region are potential hidden interferers for an $\mathbf{n}_0$ to **R** RTS frame.

One objective of carrier sensing in CSMA/CA based protocols is to avoid collisions by possibly covering all potential interferers within its (physical or virtual) CS range. Any interferer that is left uncovered is a potential hidden interferer. Obviously, VCS is not applicable for a RTS frame and hence, all potential interferers that are outside CS range of $\mathbf{n}_0$ are hidden. Such a zone containing hidden interferers for RTS frame is shown with horizontally dashed region in Fig. 3.

Note that, a transmission from an interferer located within CS range of $\mathbf{n}_0$ can also corrupt an RTS reception at $\mathbf{R}$, if such an interference signal is initiated in the same time slot in which the transmission of RTS began. Such interferers are referred to as *non-hidden* interferers. The shaded zone in Fig. 3 depicts such a zone that contains non-hidden interferers for RTS frame. Calculation of areas of the above regions as a function of S-R distance d are carried out in A.

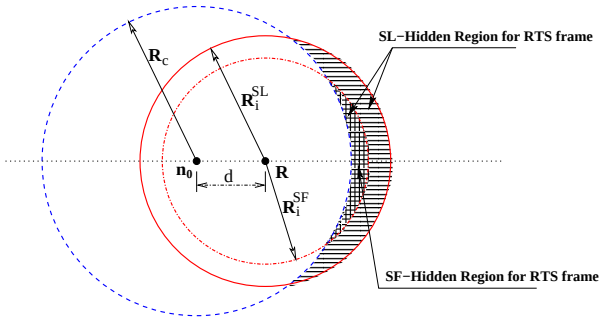

Fig. 4 Effect of ODC on the hidden region for RTS frames.

As discussed in Section 3.2, two different values of δ for SF and SL cases lead to two different interfering ranges, even for a given data rate and a given d. As shown in Fig. 4, depending upon the relative values of δ, the hidden region for an RTS frame could significantly be reduced when it is received in SF-overlapping fashion. Note that, the effect of frame arrival order dependent capture is to effectively reduce the hidden area through reduction in interference range for SF case. We will treat the two overlapping cases (SF and SL) separately in the analysis of collisions.

Now, we proceed to derive the probability of successful reception of RTS frame by considering probabilities of collisions of RTS due to hidden or non-hidden interference.

As stated in the beginning of section 4, in a network with homogeneous spatial Poisson distributed nodes with density λ, the probability of number of nodes in an area A being n is given by: $Prob(N = n) = \frac{(\lambda A)^n}{n!} e^{-\lambda A}$. Hence, if τ is the transmission probability of a node, the probability that none of the nodes in an area A initiates a transmission in a given time slot is given as:

$$Prob\{\text{No node in area A transmits in a given time slot}\}$$
$$= \sum_{k=0}^{\infty} (1-\tau)^k \frac{(\lambda A)^k}{k!} e^{-\lambda A} = e^{-\lambda \tau A} \tag{18}$$

Let A_Ω denote the area of region Ω containing hidden interferers for RTS frame. Then, from Fig. 3, $\pi R_i^2 - A_\Omega$ is the area of the region containing non-hidden interferers for RTS frame. Referring to Fig. 5, we denote A_Ψ as the area of a sub-region Ψ of the 'non-hidden-region' that also falls in the transmission range of the reference node $\mathbf{n}_0$. The areas A_Ω and A_Ψ as functions of d are computed in A.

As noted Section 4.1, a RTS frame from $\mathbf{n}_0$ will not be subjected to any non-hidden interference if none of the nodes within the area $\pi R_i^2 - A_\Omega$ initiates a transmission in the same time slot in which the RTS transmission from $\mathbf{n}_0$ has begun. Accordingly, we use different transmission probabilities, τ_R and ρ, inside and outside the transmission range of node $\mathbf{n}_0$. Denoting p_{nh} as the probability of no-collisions due to non-hidden interferers and

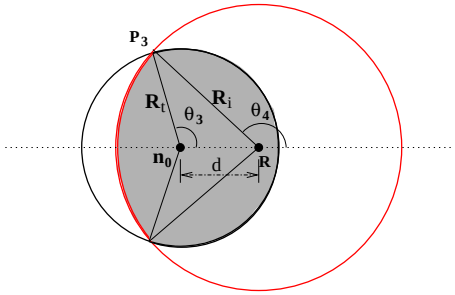

Fig. 5 The intersection of non-hidden region for RTS frames and transmission range of node n_0 is denoted as Ψ.

considering such interference as an SF case, p_{nh} as a function of S-R distance d, can be computed as:

$$\begin{aligned} & p_{nh}(d) \\ & = \sum_{k=0}^{\infty} \left[(1-\rho)^k \frac{\left(\left(\pi \left(R_i^{SF}(d) \right)^2 - A_{\Omega}^{SF}(d) - A_{\Psi}^{SF}(d) \right) \lambda \right)^k}{k!} e^{-\left(\pi \left(R_i^{SF}(d) \right)^2 - A_{\Omega}^{SF}(d) - A_{\Psi}^{SF}(d) \right) \lambda} \right] \\ & \cdot \sum_{k=0}^{\infty} (1-\tau_R)^k \frac{\left(A_{\Psi}^{SF}(d) \lambda \right)^k}{k!} e^{-\left(A_{\Psi}^{SF}(d) \right) \lambda} \\ & = e^{-\lambda \rho \left(\pi \left(R_i^{SF}(d) \right)^2 - A_{\Omega}^{SF}(d) - A_{\Psi}^{SF}(d) \right) - \lambda \tau_R A_{\Psi}^{SF}(d),} \end{aligned} \tag{19}$$

We now analyze the loss of RTS frame due to collisions with hidden interference. Fig. 6 can be used to describe the possible overlaps of RTS frame with an interfering frame F from a hidden terminal. A hidden interfering node is completely unaware of the transmission initiation from $\mathbf{n}_0$ and hence, unlike non-hidden interference, here the F can begin in any of the (vulnerable) slots such that it overlaps with the RTS frame at least in one time slot. Further note that, F could be any of the four frames (RTS, CTS, data, ACK) from the interferer. However, as both, the transmission probability and the length of CTS and ACK frames, are relatively negligible, for simplicity of the analysis we consider only two possibilities of F: RTS and data. To incorporate the effect of ODC in our analysis we need to consider the number of vulnerable slots separately for SF and SL cases.

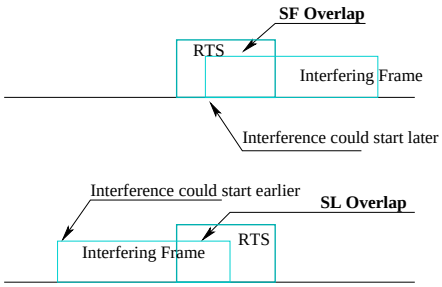

Fig. 6 Possible overlaps of a RTS frame with hidden interferences.

We denote $N_{F_1-F_2}$ as the number of vulnerable slots for an overlap between the intended signal frames F_1 and F_2 in SF and SL cases, respectively. From Fig. 6 it is clear that, in SF case the number of vulnerable slots are independent of the type of interfering frame and hence,

$$N_{RTS-F}^{SF} = \left\lceil \frac{T_{RTS}}{T_{gen}} \right\rceil, \qquad F \in \{RTS, data\}, \tag{20}$$

where $\lceil . \rceil$ is the ceiling function. On the other hand, the number of vulnerable slots in SL case will equal the number of slots in the interfering frame F. That is,

$$N_{F-RTS}^{SL} = \left\lceil \frac{T_F}{T_{gen}} \right\rceil, \qquad F \in \{RTS, data\}. \tag{21}$$

As the hidden interferer will always be located outside the transmission range from the sender, it is clear that an interfering RTS frame will be transmitted with the generic RTS-transmission probability ρ. An interfering data frame will be transmitted by a node only if it has reached its own RTS-Success state, i.e., with a transmission probability $\Pi_{RS} = \Pi_I P\{RS|I\}$.

Probability of no-collision of SF (SL) type with a frame F is same as the probability that no node in the area A_Ω^{SF} (A_Ω^{SL}) transmits frame F (with probability τ_F) in the vulnerable period N_{RTS-F}^{SF} (N_{F-RTS}^{SL}). So, $Prob\{\text{No SF-Collision of RTS with F}\}(d) = e^{-\tau_F \lambda A_\Omega^{SF}(d) N_{RTS-F}^{SF}}$, and $Prob\{\text{No SL-Collision of RTS with F}\}(d) = e^{-\tau_F \lambda A_\Omega^{SL}(d) N_{F-RTS}^{SL}}$.

Thus, the probability $p_h(d)$ that RTS is not lost due to collisions with hidden interferences is:

$$\begin{aligned} p_h(d) = Prob\{\text{No SF-Collision of RTS with RTS}\}(d) \cdot Prob\{\text{No SF-Collision of RTS with data}\}(d) \\ \cdot Prob\{\text{No SL-Collision of RTS with RTS}\}(d) \cdot Prob\{\text{No SL-Collision of RTS with data}\}(d) \end{aligned}$$

Eventually, for a successful RTS reception, it should not face any collisions due to non-hidden or hidden interference. Hence,

$$Prob\{\text{successful reception of RTS}\}(d) = Prob\{\text{no collision of RTS}\} = p_{nh}(d) p_h(d).$$

4.2.2 CTS response to a RTS

Consider the event when **R** does not respond to a successfully received RTS with a CTS. To derive the probability of this event we use an illustrative scenario of Fig. 7. A possible sequence of transmission events is shown in Fig. 8. The receiver **R** will not respond to the RTS from $\mathbf{n}_0$ if it finds its NAV non-zero at time SIFS after t_1. As shown

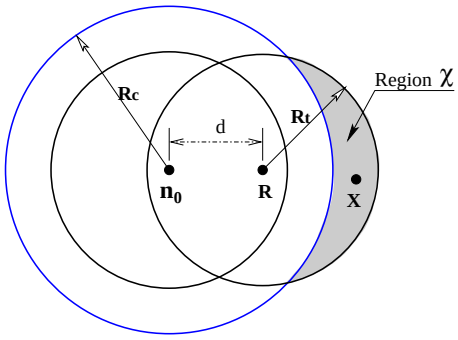

Fig. 7 Depiction of the case when a RTS from $\mathbf{n}_0$ is not responded with a CTS by **R**. **R** overheard a frame F from **X** and set its NAV. It remains non-zero when it receives a RTS from $\mathbf{n}_0$, and hence it does not respond with a CTS.

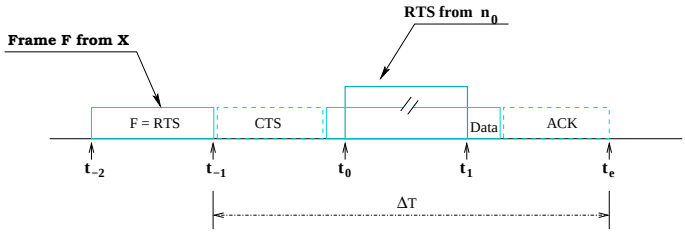

Fig. 8 Timing diagram illustrating the case of no-CTS-response where a RTS frame from **X** does not allow **R** to respond to the sender $\mathbf{n}_0$. The vulnerability period in which the RTS from node **X** may begin is $\Delta T - T_{RTS}$.

in Fig. 7, let **X** be such a node whose transmitted frame F gets the NAV of **R** loaded with a duration value ΔT which does not expire at t_1. If reception of F is completed at time t_{-1}, then for **R** to be non-responding to $\mathbf{n}_0$

$$\Delta T > (t_1 + SIFS) - t_{-1}. \tag{22}$$

It is obvious that, F from **X** and RTS from $\mathbf{n}_0$ must be received at **R** in non-overlapped fashion and hence, $t_{-1} < t_0$ where t_0 is the starting time of RTS frame from $\mathbf{n}_0$. Thus, as $t_1 - t_0 = T_{RTS}$, $t_1 - t_{-1} \geq T_{RTS}$. Therefore, the condition in (22) becomes

$$\Delta T > T_{RTS} + SIFS. \tag{23}$$

The duration value in any data frame is always equal to $T_{ACK} + SIFS$ and in any ACK frame it is always *zero*. Thus, the condition in (23) rules out the possibility of F being a data or an ACK because of very low values of ΔT in such cases. Further, we ignore the possibility of F being a *sensed-only* frame as in that case the value of ΔT would be EIFS which is almost equal to the required lower bound in (23). For example in 802.11a at 6 Mbps data rate, $EIFS = 100\mu S$ and $T_{RTS} + SIFS = 66\mu S$. Therefore, F is either a RTS or a CTS, and **X** must be located outside CS range of $\mathbf{n}_0$ but within transmission range of **R**. This leaves the remaining region χ (shaded region in Fig. 7) in which nodes like **X** may lie. For simplicity of the analysis we ignore the case where $F = CTS$ as the probability of a RTS transmission is relatively higher than that of CTS.

Fig. 8 shows the timing relationship when $F = RTS$. ΔT for a RTS frame will be $\Delta T = SIFS + T_{CTS} + SIFS + T_{data} + SIFS + T_{ACK}$, which expires at t_e. Obviously, ΔT would not expire at t_1 if following conditions are satisfied: (i) t_1 occurs after t_{-1}, (ii) t_1 occurs before t_e, (iii) t_0 occurs after t_{-1}, and (iv) t_0 occurs at least T_{RTS} before t_e. From above, it is easy to deduce that, the vulnerable period in which the transmission of F may begin is $\Delta T - T_{RTS}$. Therefore, the probability $p_{cr} = Prob\{\text{Received RTS responded with CTS}\}$ that **R** responds to $\mathbf{n}_0$ with a CTS given that it has received the RTS from $\mathbf{n}_0$ successfully is equivalent to saying that, no node in the area A_χ transmits a RTS in any of the time slots during a period of $\Delta T - T_{RTS}$. Hence p_{cr} as a function of d can be expressed as: $p_{cr}(d) = e^{-\rho\lambda A_\chi(d)\left\lceil \frac{(\Delta T - T_{RTS})}{T_{gen}} \right\rceil}$, where $\lceil\cdot\rceil$ is the ceiling function.

We denote $rtsSucc$ as the event that a transmitted RTS is responded by a successful CTS. Then,

$$\begin{aligned} Prob\{\text{rtsSucc}\}(d) &= Prob\{\text{Receiver does not transmit in next slot}\}. \\ &\quad .Prob\{\text{successful reception of RTS}\}(d) \\ &\quad .Prob\{\text{Received RTS responded with CTS}\}(d) \\ &= (1-\tau_R).p_{nh}(d).p_h(d).p_{cr}(d). \end{aligned}$$

Note that, $Prob\{\text{rtsSucc}\}(d)$ is a function of S-R distance d which is a random variable. Therefore, for all equations involving this term, we need to find an expected value based on the probability distribution (PDF) of d. Assuming that a node chooses any of its neighbors as its destination within its transmission range equi-probably, assuming 2-D Poisson distribution for the number of nodes in a given area, we obtain the PDF $f(d)$ of the distance between a node and its neighboring nodes within the transmission range R_t as: $f(d) = \frac{2d}{R_t^2}$, for $0 \leq d \leq R_t$. Hence, the average RTS frame success probability is obtained as:

$$Prob\{\text{rtsSucc}\} = \int_0^{R_t} Prob\{\text{rtsSucc}\}(x) f(x) dx.$$

4.3 Analysis of Success/Failure of Data Frame

For the derivation of transition probability for the transition from RTS-Success state to data-Success (or data-Failure) state, we need to determine the probability of receiving an ACK frame in response to a data frame. As we neglect the possibility of ACK collisions, loss of data frame in collisions is the only remaining reason due to which a transmitted data may not be acknowledged by its intended receiver. In this section, we investigate the collision vulnerability of data frame.

A data frame is said to be lost due to collision if it is received at the receiver in overlapped fashion with another frame being transmitted from within interference range of the receiver. Accordingly, all the nodes within the interference range of node **R** are potential interferers in Fig. 9. However, due to prior transmission of a RTS frame, there would not be any non-hidden interferer for the subsequent data frame. Further, the nodes within region Φ (in Fig. 9) should have received CTS from **R** successfully, and hence they would not initiate any transmission until the ACK is transmitted by **R**. Thus, the union of regions Θ_i and Θ_o is the hidden region [3] for the data frames. Further, all the nodes within region Θ_i will defer for EIFS after CTS completion, i.e., they will be hidden for a shorter (vulnerable) period. However, the nodes within region Θ_o will function as hidden terminals for a longer

[3] Note that, the area of hidden region depends on the value of CS range and the S-R separation distance d. Fig. 9 shows a typical scenario where this region is the union of the two *non-zero* sub-regions Θ_i and Θ_o.

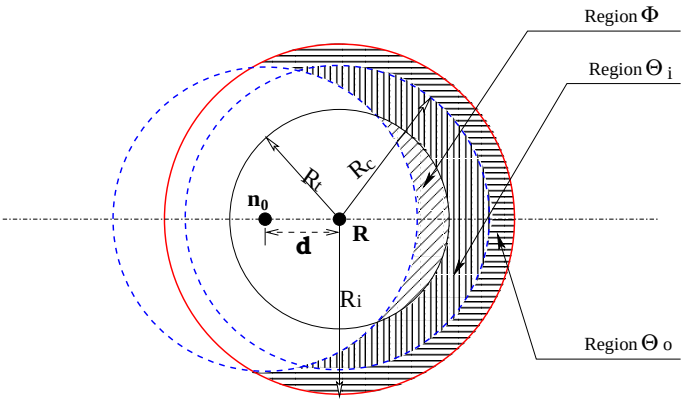

Fig. 9 The nodes within region Φ should have received CTS from **R** successfully, and hence, would no more be hidden for the subsequent data frame.

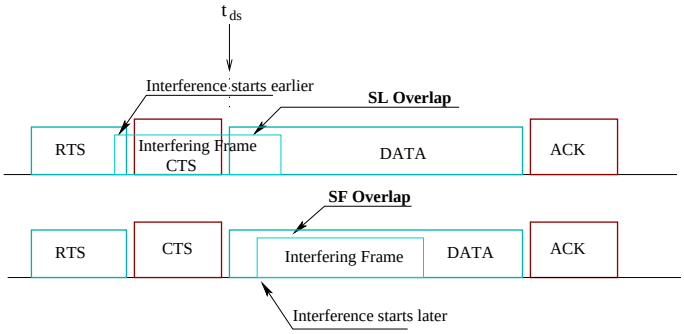

Fig. 10 Possible overlaps of data frame with hidden interferences.

vulnerable period, because a potential interfering transmitter is free to transmit at any time, which will cause interference at **R**. Calculation of areas A_{Φ}, A_{Θ_i}, and A_{Θ_o} as a function of d is carried out in A. The effect of ODC is to effectively reduce the area of hidden zone through reduction in interference range for SF case. The two overlapping cases (SF and SL) will be treated separately in the collision analysis.

Now we determine the vulnerable periods for SF and SL types of overlaps of data frame. Fig. 10 shows the SF and SL types of overlaps of data frame with interference from a hidden transmitter. For SF collision the interfering RTS frame has to start after t_{ds}. Due to EIFS mechanism the number of vulnerable slots in SF-collisions can be given as:

$$N^{SF}_{data-F} = \begin{cases} \left\lceil \frac{(T_{data}-EIFS)}{T_{gen}} \right\rceil & \text{if } \mathbf{X} \text{ is within } \Theta_i \\ \left\lceil \frac{T_{data}}{T_{gen}} \right\rceil & \text{if } \mathbf{X} \text{ is within } \Theta_o, \end{cases}$$

where $\lceil \cdot \rceil$ is the ceiling function. Note that, for SF case the number of vulnerable slots do not change with the type of interfering frame. As the transmission probability of the interfering RTS frame is larger than that of a data frame, we consider only the RTS frame as a possible source of SF-collisions. Denoting $F_{in}(F_{out})$ as the interfering frame from a node in region Θ_i (Θ_o), the data frame will not be subjected to any SF collision if none of the hidden nodes within region Θ_i (Θ_o) initiates a transmission of frame F_{in} (F_{out}) in any of the corresponding vulnerable slots. Hence,

$$\begin{aligned} Prob\{\text{no SF Collisions of data}\}(d) &= Prob\{\text{no SF Collisions of type } data - F_{in}\}(d) \\ &\quad \cdot Prob\{\text{no SF Collisions of type } data - F_{out}\}(d) \\ &= e^{\left(-\rho\lambda A^{SF}_{\Theta_i}(d) N^{SF}_{data-F_{in}}\right)} \cdot e^{\left(-\rho\lambda A^{SF}_{\Theta_o}(d) N^{SF}_{data-F_{out}}\right)}. \end{aligned}$$

As observed in Fig. 10, for qualifying as an SL-interference, the interfering frame F must have started before t_{ds}. We consider the cases of F to be either RTS or data and ignore the other two cases of it being CTS or ACK. The vulnerable number of slots can be obtained as:

$$N^{SL}_{F-data} = \begin{cases} \left\lceil \frac{T_{RTS}}{T_{gen}} \right\rceil & \text{for } F = RTS, \\ \left\lceil \frac{(T_{RTS}+SIFS+T_{CTS}+SIFS)}{T_{gen}} \right\rceil & \text{for } F = data. \end{cases}$$

$F = RTS$ is intuitive from the explanation for (20), while the value for $F = data$ needs some explanation. Given that the RTS from $\mathbf{n}_0$ was received at $\mathbf{R}$ without any collision, the transmission of F must not have started before the starting instant of RTS from $\mathbf{n}_0$. Hence, the vulnerable number of slots for $F = data$ is justified in above equation.

Next, we discuss about the possible location of an interferer causing SL type of collision to the data frame. As $T_{RTS} \approx T_{CTS}$, with very high probability, the transmission of $F = RTS$ starts after the beginning of CTS. Therefore, the location of interferer is limited within Θ_o region, as otherwise it would not have initiated its RTS. The frame $F = data$ could have started either during RTS or during CTS. If it started during RTS, the interferer could lie anywhere in Θ_i or Θ_o but outside R_i^{SF} of receiver $\mathbf{R}$. And if it started during CTS, it could lie only in region Θ_o. Thus, a region other than Θ_o from where the interference can occur is negligibly small. Hence, for simplicity of the analysis, we consider A_{Θ_o} as the area of the SL-interference zone. Accordingly,

$$\begin{aligned} Prob\{\text{no SL Collisions of data}\}(d) &= Prob\{\text{no SL Collisions of type RTS-data}\}(d) \\ &\quad .Prob\{\text{no SL Collisions of type data-data}\}(d) \\ &= e^{\left(-\rho\lambda A_{\Theta_o}^{SL}(d) N_{RTS-data}^{SL}\right)} . e^{\left(-\Pi_{RS}\lambda A_{\Theta_o}^{SL}(d) N_{data-data}^{SL}\right)}. \end{aligned}$$

Finally, denoting $dataSucc$ as the event that, given a successful exchange of RTS/CTS, the subsequent data frame reaches the intended receiver without any collisions,

$$Prob\{\text{dataSucc}\}(d) = Prob\{\text{no SF Collisions of data}\}(d).Prob\{\text{no SL Collisions of data}\}(d).$$

Based on the descriptions of various states of the model in Fig. 2, the transition probabilities $P\{RS|I\}$, $P\{RF|I\}$, $P\{D1|I\}$, and $P\{D2|I\}$ can be expressed in terms of $Prob\{\text{rtsSucc}\}$ as:

$$P\{RS|I\} = \int_0^{R_t} f(x).\tau_R.Prob\{\text{rtsSucc}\}(x)\mathrm{d}x, \tag{24}$$

$$P\{RF|I\} = \tau_R - P\{RS|I\}, \tag{25}$$

$$P\{D1|I\} = \int_0^{R_t} f(x).(1-\tau_R).(1-\tau').Prob\{\text{rtsSucc}\}(x)\mathrm{d}x, \tag{26}$$

$$P\{D2|I\} = \int_0^{R_t} f(x).(1-\tau_R).(1-\tau').\left(1 - Prob\{\text{rtsSucc}\}\,(x)\right)\mathrm{d}x, \tag{27}$$

where, in the last two equations, τ' is the probability that no node in the so called *transmission deferral zone* (denoted as κ) initiates a transmission attempt in next time slot. As the name suggests, the κ zone is the region in which a node is prevented from transmission by an on-going transmission of a data frame. Clearly, besides covering the nodes within CS range of the sender, this zone also covers the nodes within transmission range of the sender as well as that of the receiver. Nodes within transmission range will have received either a RTS or a CTS and hence will defer their own transmission due to VCS. On the other hand, the nodes within CS range of both the sender and the receiver, will be receiving each of the four frames, at least as *sensed-only* frames and hence, will be deferring their own transmission due to PCS. Nodes located exclusively within CS range of the sender such that they receive only 'sense-only' frames transmitted by the sender only (i.e., RTS and data only and not CTS and ACK), they will also defer their own transmission until the ACK reception is completed at the receiver due to PCS and EIFS mechanism. However, the nodes that are located exclusively within CS range of the receiver such that they receive only 'sense-only' frames transmitted by the receiver only (i.e., CTS and ACK only and not RTS and data) will defer their transmission but for a limited time (EIFS) after each of the overheard frame. And hence, we do not include such nodes in the transmission deferral zone. Denoting the area of transmission deferral zone as A_κ, τ' can be expressed as:

$$\tau' = e^{(-\tau_R \lambda A_\kappa)}.$$

Thus, the term $(1-\tau')$ in (26) and (27) stands for $\mathbb{P}$(at least one node in the CS range transmits) to cause the transition of node $\mathbf{n}_0$ from Idle state to a Deferring state. Now, we have six equations ((12), (16), (17), (24), (26), and (27)) with six unknowns (p_{ii}, Π_I, T_{gen}, $P\{RS|I\}$, $P\{D1|I\}$, and $P\{D2|I\}$). This system of non-linear equations can be solved to find the values of all these six parameters for given values of λ and R_c.

As we have neglected the ACK collisions, the transition probability $P\{DS|RS\}$ becomes:

$$P\{DS|RS\} = \int_0^{R_t} f(x) Prob\{\text{dataSucc}\}(x)\mathrm{d}x,$$

and hence,

$$P\{DF|RS\} = 1 - P\{DS|RS\}.$$

Having determined the steady state probability Π_I, other steady state probabilities can be found easily from equations (7a) to (7f).

Let TH_n denote the throughput per user, defined as the successfully transmitted average payload by an arbitrary user in a generic time slot, which is given by

$$TH_n = \frac{\Pi_{DS} L_{dt}}{T_{gen}}, \tag{28}$$

where, L_{dt} is the (constant) length of all data frames in bits.

5 Validation of the Model

In this section, we validate the analytical model through ns2 simulations. We noted that, the default IEEE 802.11 MAC implementation in ns2 does not support the scenarios where the interfering range is greater than the CS range. After incorporating the necessary changes to accommodate $R_i > R_c$ cases, the MAC and PHY layer codes were modified to incorporate ODC at PHY.

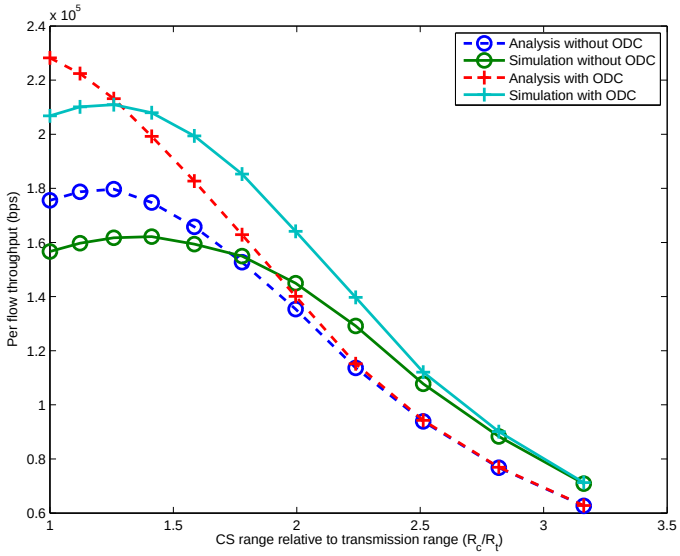

Fig. 11 Validation of analysis: Per flow throughput versus R_c/R_t ratio at 6 Mbps data rate.

Further modifications were carried out in ns2 to reflect the corresponding assumptions in the analysis. The network topology and other system parameters chosen to match the parameters for analytical results were: Fixed CW of 1024 system slots with no retransmission; fixed MAC data payload size 1018 Bytes; 6 Mbps data rate for control packets and 6, 9, 12, 18, 24, 36, 48, and 54 Mbps data rates for data packets. Nodes were randomly deployed in an area of 2000 m $\times$ 2000 m with node density of $\lambda = 5 \times 10^{-5}$ nodes/m^2. This corresponds to around 9 to 10 nodes within a transmission radius of 250m. Every node arbitrarily selects one of its R_t-neighbors (1-hop) as a receiver if it finds at least one. CBR traffic was generated from upper layer using UDP at the transport layer. At routing layer NO-Ad-Hoc (NOAH) protocol [2] was used with Time-To-Live set to 1. The choice of UDP at transport layer and NOAH at routing layer guarantees no reactions from higher layers for the happenings at the MAC layer. The chosen rate of CBR traffic is sufficient to keep the node always backlogged at the link layer. Both, the short and long retry limits were made 1 and the binary exponential back-off was stopped and a fixed contention window was used. Though, (almost) all the nodes are active transmitters, in calculating the throughput we consider only those sender-receiver pairs that are within the inner square of 1000 m $\times$ 1000 m to avoid boundary effects.

Fig. 11 shows the per node throughput versus R_c/R_t ratio at 6 Mbps data rate with and without ODC. Though the simulation and analysis curves do not match at well, the trend is more or less the same. It can be noted that, the

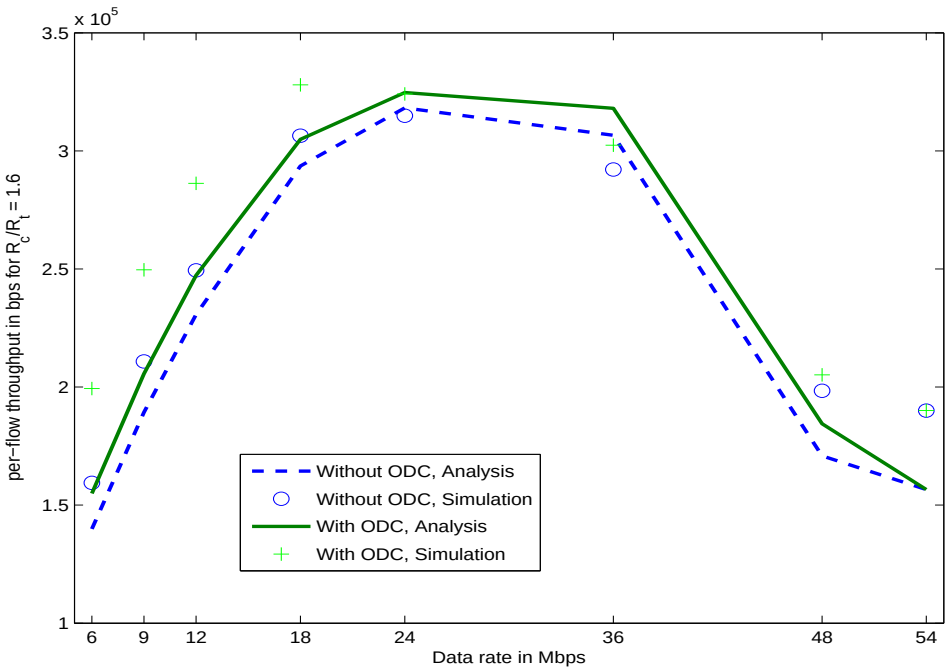

Fig. 12 Validating the analytical model at higher data rates: The plots are for typical value of $R_c/R_t = 1.6$. We have verified at other values of R_c/R_t as well.

difference between simulation and analysis is higher when R_c/R_t is lower. We analyzed the reason and found the following: Many of earlier analytical works (e.g., the seminal work in [5]) assume that, all nodes are within the CS range of every other node in the system, and hence, the transmission probability of every node is the same as every node senses the same environment around itself. However, this assumption of uniform transmission probability is no more valid with the increase in the separation between two nodes and/or with the reduction in the CS range. As discussed in Section 4.1 (ref. (13) and (14)), we addressed this problem by assuming two different transmission probabilities, pw and ρ, for nodes within transmission range and for those nodes outside transmission range (but within CS range), respectively. However, this also, not being entirely accurate, does not work well when CS range is small. The accurate analysis is found to be difficult [7] and most existing analysis [32], [17] assume constant transmission probability for all nodes in the system. The focus of our work is on the effect of ODC on deciding the CS threshold which is brought out by the trends shown in Fig. 11.

To validate the analysis at higher speeds, further analysis and simulation are carried out at higher data rates of IEEE 802.11a. Fig. 12 shows per-flow throughput at a typical value of R_c/R_t (= 1.6) with different data rates. Here also, though the analysis does not match exactly, the trend is more or less the same.

6 Impact of ODC on the Choice of CS Threshold

In this section, we use the analytical model developed in section 4 to evaluate the impact of ODC on the choice of optimum CS threshold. As the significance of ODC diminishes with increase in operating data rates, we expect the gain due to ODC also to reduce with increase in data rate. To see this effect we plot and discuss the analytical results at various data rates of IEEE 802.11a. The system parameters considered are as follows: CW size: 1024 and 128 system slots, with no retransmission option; node density λ: 5×10^{-5}, 1×10^{-4} nodes/m^2; fixed MAC payload size 1018 Bytes; rate for control packets: 6 Mbps (802.11**a** basic rate for RTS, CST, ACK); rate for data frames: 6, 9, 12, 18, 24, 36, 48, 54 Mbps (802.11**a** data rates). Reduction in exposed terminals results in enhanced network throughput while possibly increasing the number of frame losses due to the increase in the number of hidden terminals. Therefore, following two performance metrics become important for evaluating the trade-off involved: per user throughput and frame loss rate. Per user throughput was already derived in (28). Using the notation Π_{DF} for steady state probability of DF state, the data frame loss rate (FLR) can be obtained as:

$$FLR = \frac{\Pi_{DF}}{\Pi_{DS} + \Pi_{DF}} = \frac{P\{DF|RS\}}{P\{DS|RS\} + P\{DF|RS\}}.$$

As our interest is to see the impact of ODC on the optimality of CS threshold, we plot the above performance metrics against different values of R_c for different data rates of IEEE 802.11a.

Impact of ODC on CS threshold at different data rates: Figs. 13 and 14 respectively show frame loss rate and average per-node throughput versus R_c/R_t for a fixed CW 128 slots and node density of 5×10^{-5} (which corresponds to around 10 nodes in $R_t = 250$ m). Both the figures show results at four representative data rates (Mbps) of 802.11a: 6, 18, 36, and 54, with and without ODC.

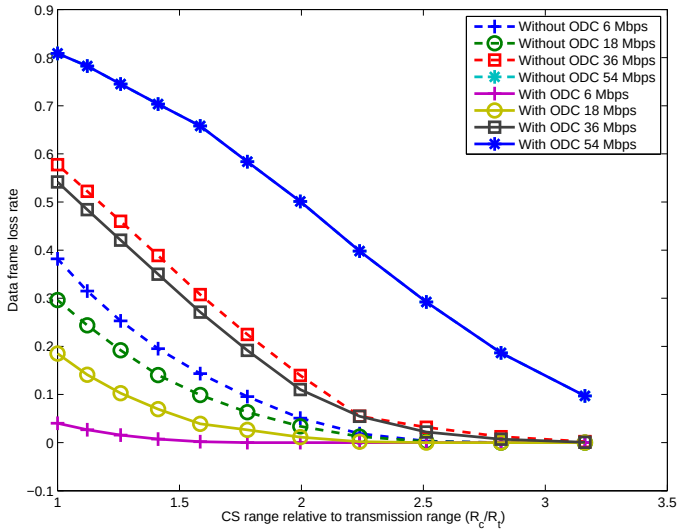

Fig. 13 Frame loss rate for data frames versus normalized CS range. CW = 128 and $\lambda = 5 \times 10^{-5}$ nodes/m^2.

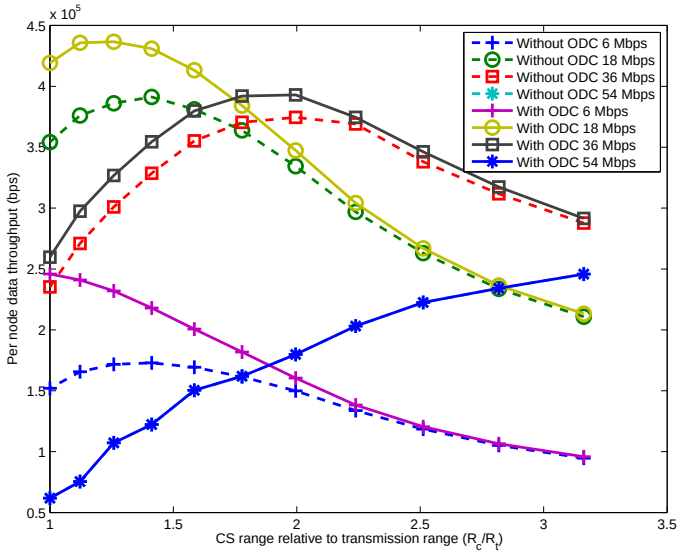

Fig. 14 Per-node throughput versus normalized CS range. CW = 128 and $\lambda = 5 \times 10^{-5}$ nodes/m^2.

As discussed in Section 4.3, at low data rates, the number of SL collision of data frames is reduced due to VCS, while the number of SF collisions are less due to the lower value of capture threshold in SF case (δ^{SF}). This has resulted in significant reduction in frame loss rate at low data rates (up to 18 Mbps) with ODC, as observed in Fig.13. Though the frame loss rate plots show almost monotonic decreasing trend due to reduction in interference with the R_c/R_t, the throughput curves show a very different trend with an optimum R_c/R_t. This is due to the fact that, hidden terminals dominate towards lower value of R_c/R_t (i.e., $= 1.0$) while exposed terminals dominate

towards higher value of R_c/R_t (i.e., $= 3.5$). In other words, a lower value of R_c leads to the improvement in spatial reuse through reduction in exposed terminals while increasing the probability of collision due to increased number of potential hidden terminals. The impact of ODC is clear from the throughput curves of Fig. 14 as well. At low data rates there is a shift in the optimum PCS threshold. As the data rate increases beyond 18 Mbps, the difference between δ^{SF} and δ^{SL} (cf. Table 1) reduces, and so the difference between the two corresponding curves (with and without ODC) also becomes small. At 54 Mbps, the performance graphs for the two cases overlap as the difference between the corresponding capture thresholds becomes null.

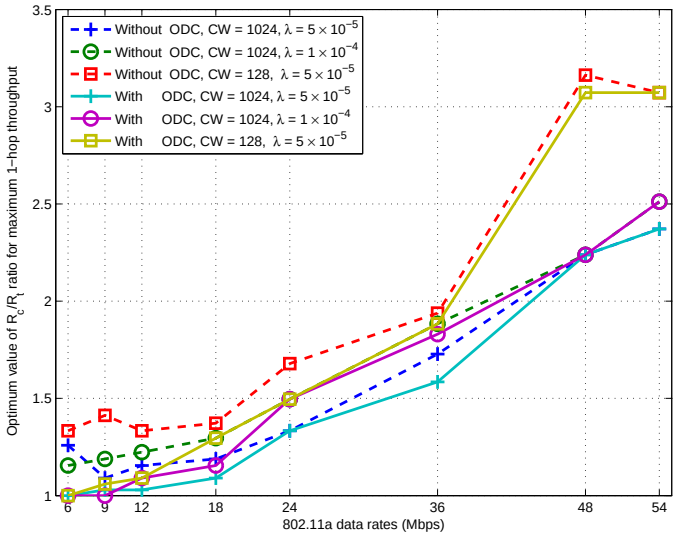

Fig. 15 Optimum value of R_c/R_t versus different data rates of 802.11a for different combinations of CW and λ.

To study the impact of ODC on the amount of shift in optimum PCS threshold, we obtain the optimum value of R_c/R_t ratio for which the throughput is maximum at different data rate. Fig. 15 shows these results with and without ODC for different combinations of λ and CW. The significant impact of ODC in low data rate region can be observed in all the curves.

Study of multihop network performance

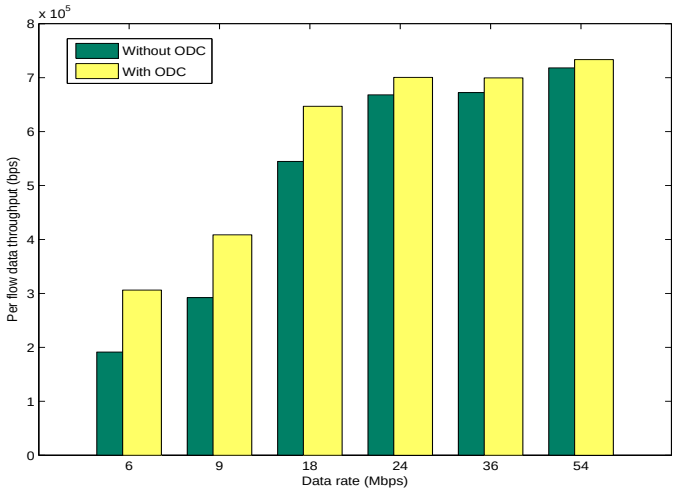

Fig. 16 Simulated multihop network performance at different data rates of IEEE 802.11a.

While the numerical results serve the purpose of mathematical demonstration of the effect of ODC on the choice of CS threshold, it involves assumptions that relaxes some practical network parameters. Hence, we further conducted simulation based network performance evaluation by considering more realistic system parameters. Further, though the optimum value of carrier sense range shifts from its value in single hop networks to multihop networks [29], the effect of ODC should be prevailing irrespective of number of hops in a flow. To verify this intuition we chose multihop networks for further evaluations.

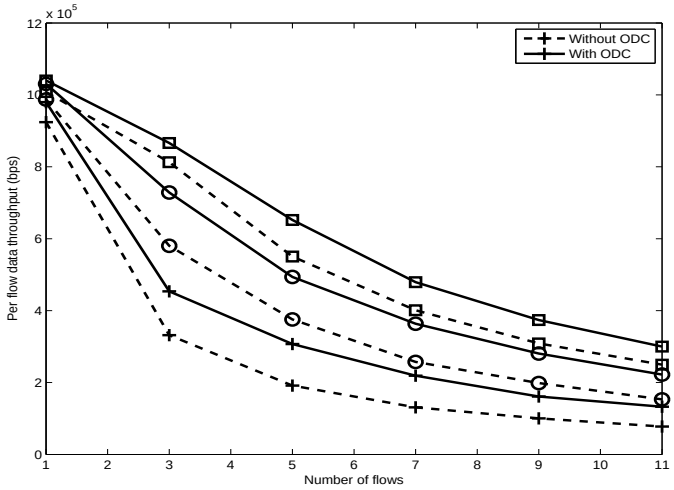

Fig. 17 Simulated multihop network performance for different number of flows.

To avoid excessively high run time, we had to reduce the network size. We deployed 80 nodes in an area of 1250m $\times$ 1250m, which corresponds to around 10 nodes in a transmission range of 250m. n number of flows were established between arbitrarily chosen sender-receiver pairs, with end-to-end source-destination distance randomly selected 500m to 600m. We used AODV routing protocol which tries to establish a route with minimum number of hops, and hence, the above end-to-end source-destination separation corresponds to around 3 hops. Each of these flows was sourced with a CBR traffic at the application layer, offering fixed sized packets of 1000 bytes. Standard back-off algorithm with CW in the range of 15 to 1023 was used with short and long retry limits set to 7 and 4 respectively. The CS threshold was set such that, R_c/R_t is set to the optimum values for 'with ODC' case for CW = 128 and $\lambda = 5 \times 10^{-5}$ from Fig. 15 for the respective data rates. Each data point was generated by taking an average of 50 simulation runs.

Fig. 16 shows per flow throughput at various data rates of 802.11a. As observed in single hop network performance, in multihop network scenario as well, the performance gain with ODC decreases at higher data rates. For example, the plots in Fig. 16 affirm that, with ODC the gain in per flow throughput are respectively around 60%, 40%, 19%, 5%, 4%, and 2% at 6, 9, 18, 24, 36, and 54 Mbps data rates. The reason for decreased gain at higher data rates is due to reduced difference in arrival order dependent capture threshold.

Fig. 17 shows per flow throughput versus number of flows for data rates up to 18 Mbps. It can be observed that, the gain with ODC increases from 6%, 4%, and 3% to 71%, 45%, and 20% at 6 Mbps, 12 Mbps, and 18 Mbps, respectively, when number of simultaneous network flows increases from 1 to 11. Here, the increase in the number of flows leads to an increased interference due to higher network activities. This results into increasing positive effect of ODC exploitation up to 7 number of flows, after which the gain tends to saturate.

7 Concluding Remarks

In this paper, we have developed a 7-state model to analytically capture the network performance of RTS/CTS enabled IEEE 802.11 DCF network with the nodes having ODC capability. Validation of the analytical model has been carried out through ns2 simulations after incorporating appropriate changes to accommodate the ODC capability of the nodes.

Utilizing the developed analytical framework, we have investigated the impact of considering ODC capability on the optimal choice of CS range in IEEE 802.11a wireless ad hoc networks with decentralized control. With the

optimal CS range, the throughput performance gain up to moderately high data rates has been shown to be quite significant – up to 41%. Since the order-dependence of capture threshold is less prominent at higher data rates, correspondingly the performance gain with ODC is also reduced.

A Derivation of different areas

A.1 Area of Hidden Region for RTS Frames: A_Ω

A_Ω refers to the area of the horizontal-dashed region in Fig. 3. Let d_0 and d_1 be defined as: $d_0 = \frac{R_c}{K+1}$ and $d_1 = \frac{R_c}{K-1}$. Then, the hidden area for RTS frames can be obtained as:

$$A_\Omega(d) = \begin{cases} 0 & \text{for } 0 \le d \le d_0 \\ \theta_2(d)R_i^2(d) - \theta_1(d)R_c^2 + 2A_{\triangle(n_0RP_1)} & \text{for } d_0 < d \le \min(d_1, R_t) \\ \pi\left(R_i^2(d) - R_c^2\right) & \text{for } d_1 < d \le R_t, \end{cases} \tag{A.1}$$

where, $\theta_1(d)$, $\theta_2(d)$, and $A_{\triangle(n_0RP_1)}$ are derived as follows:

$$\theta_1(d) = \cos^{-1}\left(\frac{R_c^2 + d^2 - R_i^2(d)}{2R_c d}\right) \text{ and } \theta_2(d) = \pi - \cos^{-1}\left(\frac{d^2 + R_i^2(d) - R_c^2}{2dR_i(d)}\right).$$

Denoting $s(d) = \frac{R_c + R_i(d) + d}{2}$, we get

$$A_{\triangle(n_0RP_1)} = \sqrt{s(d)(s(d) - R_c)(s(d) - R_i(d))(s(d) - d)}\,.$$

A.2 Area of Non-hidden Region for RTS Frames Covered by the Transmission Range of Sender: A_Ψ

Refer to Fig. 5. Let $d_2 = \frac{R_t}{K+1}$ and $d_3 = \frac{R_t}{K-1}$. Then,

$$A_\Psi(d) = \begin{cases} \pi R_i^2(d) & \text{for } 0 \le d \le d_2 \\ \pi R_i^2(d) - \theta_4(d)R_i^2(d) + \theta_3(d)R_t^2 & \\ \quad -2\sqrt{s(d)(s(d) - R_t)(s(d) - R_i(d))(s(d) - d)} & \text{for } d_2 < d \le \min(d_3, R_t) \\ \pi R_t^2 & \text{for } d_3 < d \le R_t \end{cases} \tag{A.2}$$

where, $s(d) = \frac{R_t + R_i(d) + d}{2}$ and $\theta_3(d)$ and $\theta_4(d)$ are calculated as follows:

$$\theta_3(d) = \cos^{-1}\left(\frac{R_t^2 + d^2 - R_i^2(d)}{2R_t d}\right) \text{ and } \theta_4(d) = \pi - \cos^{-1}\left(\frac{d^2 + R_i^2(d) - R_t^2}{2dR_i(d)}\right),$$

A.3 Area of Hidden Region for Data Frames: A_Θ

Referring to Fig. 9, $A_\Theta = A_\Omega - A_\Phi$, where A_Φ ($= A_\chi$, discussed in Section 4.2.2) is non-zero only if $d > R_c - R_t$ and its derivation is similar to that of A_Ω in (A.1). The hidden area for the data frames A_Θ has two sub-regions A_{Θ_i} and A_{Θ_o}. Let $d_c = \frac{R_c}{K}$. The area of A_{Θ_i} can be determined as:

$$A_{\Theta_i} = \begin{cases} A_\Theta & \text{for } d \le d_c \\ \pi R_c^2 - A_\Upsilon & \text{for } d > d_c, \end{cases} \tag{A.3}$$

where A_Υ is the area of intersection of two circles having same radius R_c whose centers are d distance apart. It is given by: $A_\Upsilon = 2R_c^2\cos^{-1}\left(\frac{d}{2R_c}\right) - \frac{1}{2}d\sqrt{4R_c^2 - d^2}$. Finally, A_{Θ_o} is derived as:

$$A_{\Theta_o} = \begin{cases} 0 & \text{for } d \le d_c, \\ A_\Theta - A_{\Theta_i} & \text{for } d > d_c. \end{cases} \tag{A.4}$$

References

[1] Atheros Communications. URL http://www.atheros.com/
[2] NO Ad-Hoc Routing Agent (NOAH). URL http://icapeople.epfl.ch/widmer/uwb/ns-2/noah/
[3] VINT Group: Network simulator ns-2 (version 2.33). URL http://www.isi.edu/nsnam/ns.
[4] IEEE std 802.11: Wireless LAN Medium Access Control (MAC) and Physical Layer (PHY) Specs. (2007)
[5] Bianchi, G.: Performance analysis of the IEEE 802.11 distributed coordination function. IEEE J. Sel. Areas in Commun. **18**(3), 535–547 (2000)
[6] Deng, J., Liang, B., Varshney, P.: Tuning the carrier sensing range of IEEE 802.11 MAC. In: Proc. IEEE GLOBECOM. Dallas, USA (2004)

[7] He, J., Kaleshi, D., Munro, A., Wang, Y., Doufexi, A., McGeehan, J., Fan, Z.: Performance investigation of IEEE 802.11 MAC in multihop wireless networks. In: Proc. ACM MSWIM. Montreal, Quebec, Canada (2005)
[8] Jiang, L.B., Liew, S.C.: Hidden-node removal and its application in cellular WiFi networks. IEEE Trans. Veh. Technol. **56**(5), 2641–2654 (2007)
[9] Kim, T.S., Lim, H., Hou, J.C.: Improving spatial reuse through tuning transmit power, carrier sense threshold, and data rate in multihop wireless networks. In: Proc. ACM MOBICOM. Los Angeles, CA, USA (2006)
[10] Kochut, A., Vasan, A., Shankar, A., Agrawala, A.: Sniffing out the correct physical layer capture model in 802.11b. In: Proc. IEEE ICNP. Berlin, Germany (2004)
[11] Lee, J., Kim, W., Lee, S.J., Jo, D., Ryu, J., Kwon, T., Choi, Y.: An experimental study on the capture effect in 802.11a networks. In: Proc. ACM WinTECH. Montreal, Quebec, Canada (2007)
[12] Lee, J., Ryu, J., Lee, S.J., Kwon, T.T.: Improved modeling of IEEE 802.11a PHY through fine-grained measurements. Elsevier Computer Networks **54**, 641–657 (2010)
[13] Lee, J., Kang, Y-M., Lee, S., Kim, C-K.: Opportunities of MIM capture in IEEE 802.11 WLANs: analytic study. In: Proc. ACM ICUIMC. Seoul, Korea (2011)
[14] Li, Z., Nandi, S., Gupta, A.K.: ECS: An enhanced carrier sensing mechanism for wireless ad hoc networks. Elsevier Computer Commun. **28**(17), 1970–1984 (2005)
[15] Lin, T.Y., Hou, J.: Interplay of spatial reuse and SINR-determined data rates in CSMA/CA-based, multi-hop, multi-rate wireless networks. In: Proc. IEEE INFOCOM (2007)
[16] Lu, J., Whitehouse, K.: Flash flooding: Exploiting the capture effect for rapid flooding in wireless sensor networks. In: Proc. IEEE INFOCOM. Rio de Janeiro, Brazil (2009)
[17] Ma, H., Alazemi, H., Roy, S.: A stochastic model for optimizing physical carrier sensing and spatial reuse in wireless ad hoc networks. In: Proc. IEEE MASS. Washington DC, USA (2005)
[18] Ma, H., Shin, S.Y., Roy, S.: Optimizing throughput with carrier sensing adaptation for IEEE 802.11 mesh networks based on loss differentiation. In: Proc. IEEE ICC. Glasgow, UK (2007)
[19] Ma, H., Vijayakumar, R., Roy, S., Zhu, J.: Optimizing 802.11 wireless mesh networks based on physical carrier sensing. IEEE/ACM Trans. Networking **17**(5), 1550–1563 (2009)
[20] Ma, Q., Liu, K., Miao, X., Liu, Y.: Opportunistic concurrency: A MAC protocol for wireless sensor networks. In: Proc. IEEE DCOSS. Barcelona, Spain (2011)
[21] Manweiler, J., Santhapuri, N., Sen, S., Roy Choudhury, R., Nelakuditi, S., Munagala, K.: Order matters: transmission reordering in wireless networks. In: Proc. ACM MOBICOM. Beijing, China (2009)
[22] Rappaport, T.: Wireless Communications: Principles and Practice, 2 edn. Prentice Hall (2001)
[23] Santhapuri, N., Nelakuditi, S., Choudhury, R.R.: On spatial reuse and capture in ad hoc networks. In: Proc. IEEE WCNC. Las Vegas, USA (2008)
[24] Thorpe, C., Murphy, S., Murphy, L.: IEEE 802.11k enabled adaptive carrier sense management mechanism (kapcs2). In: Proc. IFIP/IEEE Intl. Symposium on Integrated Network Management (IM). Dublin, Ireland (2011)
[25] Vegad, M.M., De, S., Lall, B.: Reconsideration of carrier sensing range for wireless ad hoc networks. In: Proc. IEEE ANTS. New Delhi, India (2009)
[26] Xu, K., Gerla, M., Bae, S.: How effective is the IEEE 802.11 RTS/CTS handshake in ad hoc networks. In: Proc. IEEE GLOBECOM. Taipei, Taiwan (2002)
[27] Yang, X., Vaidya, N.: On physical carrier sensing in wireless ad hoc networks. In: Proc. IEEE INFOCOM (2005)
[28] Ye, F., Yi, S., Sikdar, B.: Improving spatial reuse of IEEE 802.11 based ad hoc networks. In: Proc. IEEE GLOBECOM. San Francisco, USA (2003)
[29] Zhai, H., Fang, Y.: Physical carrier sensing and spatial reuse in multirate and multihop wireless ad hoc networks. In: Proc. IEEE INFOCOM (2006)
[30] Zhang, Y., Assi, C., Alawieh, B., Alazemi, H.: A spatiotemporal contention resolution for enhancing spatial reuse in wireless networks. IEEE Trans. Veh. Technol. **60**(2), 680–691 (2011)
[31] Zhu, J., Guo, X., Yang, L., Conner, W.: Leveraging spatial reuse in 802.11 mesh networks with enhanced physical carrier sensing. In: Proc. IEEE ICC. Paris, France (2004)
[32] Zhu, Y., Zhang, Q., Niu, Z., Zhu, J.: On optimal QoS-aware physical carrier sensing for IEEE 802.11 based WLANs: Theoretical analysis and protocol design. IEEE Trans. Wireless Commun. **7**(4), 1369–1378 (2008)